Superlattices and Microstructures 125 (2019) 205–213

Contents lists available at ScienceDirect

Superlattices and Microstructures

journal homepage: www.elsevier.com/locate/superlattices

Electronic properties and optical behaviors of bulk and monolayer ZrS_2: A theoretical investigation

Tuan V. Vu[a,b], A.A. Lavrentyev[c], Doan V. Thuan[d], Chuong V. Nguyen[e], O.Y. Khyzhun[f], B.V. Gabrelian[g], Khanh C. Tran[h], Hai L. Luong[i], Pham D. Tung[j], Khang D. Pham[a,b], Phuc Toan Dang[a,b], Dat D. Vo[a,b,*]

[a] Division of Computational Physics, Institute for Computational Science, Ton Duc Thang University, Ho Chi Minh City, Vietnam
[b] Faculty of Electrical & Electronics Engineering, Ton Duc Thang University, Ho Chi Minh City, Vietnam
[c] Department of Electrical Engineering and Electronics, Don State Technical University, 1 Gagarin Square, 344010 Rostov-on-Don, Russian Federation
[d] NTT Hi-Tech Institute, Nguyen Tat Thanh University, Ho Chi Minh City, Vietnam
[e] Department of Materials Science and Engineering, Le Quy Don Technical University, Ha Noi, Vietnam
[f] Frantsevych Institute for Problems of Materials Science, National Academy of Sciences of Ukraine, 3 Krzhyzhanivsky Street, UA-03232 Kyiv, Ukraine
[g] Department of Computational Technique and Automated System Software, Don State Technical University, 1 Gagarin Square, 344010 Rostov-on-Don, Russian Federation
[h] Faculty of Materials Science and Technology, University of Science, Vietnam National University Ho Chi Minh City, 227 Nguyen Van Cu, District 5, Ho Chi Minh City, Vietnam
[i] Department of Physics, Ho Chi Minh City University of Education, Ho Chi Minh City, Vietnam
[j] Department of Aerospace Technology and Equipment, Le Quy Don Technical University, Ha Noi, Vietnam

ARTICLE INFO

Keywords:
Monolayer ZrS_2
Strain
Band structure
Optical properties
First-principles

ABSTRACT

In this paper, we study the difference in electronic and optical properties of bulk and monolayer zirconium sulfide by applying the APW + lo method in the framework of density functional theory. All calculation is performed at the energy level of visual light and higher ranging from 0 eV to 15 eV. Our results demonstrates that except for the underestimated band gap like other GGA calculation, the remain properties like dielectric function, the reflectivity, absorption and loss energy are close to experiment. The valence band is constructed by mainly sulfur *s/p*-states and the lower portion of zirconium *s/p/d*-states. The conduction band is mostly donated by zirconium *d*-state. In contrast with bulk structure, the valence band maximum in monolayer has the triple peak at Γ point, making its monolayer be more sensitive to light absorption. The dielectric function has the highest peak at about 1.5–2.5 eV with remarkable anisotropy, beyond this level to the ultraviolet region the anisotropy decreases and almost disappears at energy larger than 10 eV. The absorption is at 106 x $10^4 cm^{-1}$ for energy range 5–10 eV, while the reflectivity is at its highest value of 30 %–50 % in the energy range from 0 to 8 eV. The energy loss of monolayer is higher than those of bulk. For optical and electronic properties, the monolayer show sharper peaks and their clear separation indicate the progressive application of monolayer zirconium sulfide.

* Corresponding author. Division of Computational Physics, Institute for Computational Science, Ton Duc Thang University, Ho Chi Minh City, Vietnam.
E-mail addresses: vuvantuan@tdtu.edu.vn (T.V. Vu), chuongnguyen11@gmail.com (C.V. Nguyen), khyzhun@ipms.kiev.ua (O.Y. Khyzhun), voduydat@tdtu.edu.vn (D.D. Vo).

https://doi.org/10.1016/j.spmi.2018.11.008
Received 30 September 2018; Received in revised form 5 November 2018; Accepted 9 November 2018
Available online 15 November 2018
0749-6036/

1. Introduction

Graphene, a two-dimensional sp^2-hydridized carbon monolayer has recently received considerable attention due to its extraordinary physical and chemical properties [1–3]. However, the lack of a sizable band gap has limited its application [2]. This obstacle triggers increasingly studies on new generation of graphene-like materials with suitable band gap for vast variety of application [4–6]. Recently, two-dimensional (2D) transition-metal dichalcogenides (TMDs) materials have been widely studied owing to their outstanding properties such as high carrier mobility and on/off ration [7–13]. Most of 2D TMDs materials are semiconductors with the band gap of about 2 eV which can be controlled by strains [14–17], pressure [18,19], or electric field [20–22], making them suitable for application in nanoelectronics and optoelectronics.

More recently, 2D ZrS_2, one of the TMDs group has been successfully synthesized experimentally [23], making it potential candidate for application in next-generation nanodevices such as in hydrogen storage and large scale solar cell [24–27]. Nowadays, numerous nanodevices based on the ZrS_2 such as photodetectors, field-effect transistors have been experimentally fabricated [24,28]. These findings indicated that the ZrS_2-based nanodevices demonstrated high sheet current densities up to 800–8000 $\mu A//\mu m$ with the ultrafast response of ~2 μs and ultrahigh responsivity of 7.1×10^5 AW^{-1}.

It should be noted that for most TMDs, the photoconductivity can be affected by the band structure feature [29,30]. The appropriate band gap of ZrS_2 monolayer about 2 eV is theoretically proved to maximize the absorption portion of the sunlight for water splitting [27,31], optoelectronic applications and in devices for energy harvesting [32,33] and High-performance Schottky solar cells [25]. Meanwhile, the theoretical prediction of solar hydrogen production is higher than the measured values [27,34]. However, application of ZrS_2 in optical areas has gained more interest since its band gap energy is found to be tunable by strain [35,36], by structural dimension in which the gap energy may vary from 1.7 eV [30,37] in bulk to 1.94 eV, 1.97 eV and 2.01 eV [35,38] with decreasing the structural dimension to trilayer, bilayer, and monolayer ZrS_2, respectively. The gap energy can also be varied by the vertical electric field [39]. In addition, the empty d valence band of ZrS_2 motivate the study of its ferromagnetic properties for spintronic applications [40]. This also encourages researchers to modify the gap energy of ZrS_2-based material by attaching other semiconductors, transition metal, and non-metal [34,41–43]. Despite the advantages of 2D ZrS_2-based materials, their further developments and applications are restricted by the current lack of systematic studies and comparison to analyze the difference between bulk and monolayer ZrS_2, especially at energy region higher than visual light.

Therefore, in this work, DFT approach is applied to compare the properties of bulk and monolayer ZrS_2 including electronic and optical properties for energy ranging from 0 eV to 15 eV. The relationship between electronic structure and optical behavior is also analyzed in details.

2. Theoretical model and method

The optical and electronic properties of bulk and monolayer zirconium sulfide is analyzed by employing the APW + lo method as implemented in the WIEN2k program [44]. For the full potential approximation, the non-overlapping muffin-tin sphere radii of Zr and S atoms in the ZrS_2 system are chosen to be 2.45 a.u. and 2.11 a.u., respectively. The wave function expansion for the inner region of the atomic spheres is controlled by the orbital quantum number $l_{\max} = 10$, for the interstitial region the expansion is considered by k-point so that $R_{\min}^{MT} k_{\max} = 7$. The charge density is represented by Fourier expansion with largest vector $G_{\max} = 12$ $(\text{a.u.})^{-1}$. The above parameters are chosen based on the convergence and accuracy of electronic and optical values of testing structures before using for further studying on bulk and monolayer ZrS_2. The Perdew-Burke-Ernzerhof generalized gradient approximation (PBE-GGA) potential is used for the exchange-correlation functional [45,46]. The sampling of Brillouin zone is performed using tetrahedron method of Blöchl et al. [47] and 1000 **k**-points within the full zone. The self-consistent process is considered to be converged when the difference in out-put values between the two consecutive iterations is less than 0.0001 Ry. The weak van der Waals interactions between layers of bulk ZrS_2 were described in Grimme's DFT-D3 method.

3. Results and discussion

3.1. Atomic structure and electronic property of bulk and monolayer ZrS_2

In Fig. 1, we display the crystal structure of ZrS_2, which has hexagonal rings with triple (S—Zr—S) layers. The Zr atoms are inside nearly octahedrons created by six S atoms, while the S atoms are surrounded by three Zr atoms which form trigonal pyramid-liked structure. The simulation of monolayer ZrS_2 is realized by setting the vertical parameter of the unit cell to be over 20 Å to avoid layer interaction due to the repetition of the unit cell. After geometric optimization, the relaxed lattice constants of ZrS_2 monolayer and bulk are 3.718 Å and 3.681 Å, respectively. The lattice constant of bulk ZrS_2 is in good agreement with the previous theoretical value of 3.64 Å [48,49] and the experimental measurement is 3.66 Å [37]. Meanwhile, the previous lattice constant for bilayer ZrS_2 is 3.72 Å [50]. Due to the reduction of dimensionality from bulk to monolayer, an obvious structure relaxation is expected for the absence of van der Waals interlayer interaction in monolayer, which appears to be planar structure, and thus the lattice parameter a of the ZrS_2 monolayer is slightly larger than that in bulk form. On the other hand, the distance between Zr and S atoms are nearly the same of about 2.58 Å, which also is in consistent with the experimental values [37].

We now consider the electronic properties of both the ZrS_2 bulk and monolayer, as shown in Fig. 2(a and b). It is obvious when the dimensionality of ZrS_2 decreases from 3D to 2D, the gap energies are still indirect with the conduction band minimum at the L point and the valence band maximum at the Γ point. However, the valence band maximum in the ZrS_2 monolayer is separated into two

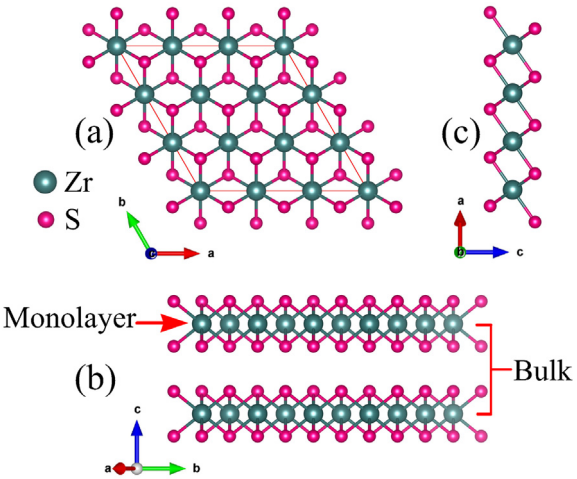

Fig 1. Atomic structure of ZrS_2: (a) top view and (b) side view of monolayer ZrS_2 respectively, (c) side view of bulk ZrS_2.

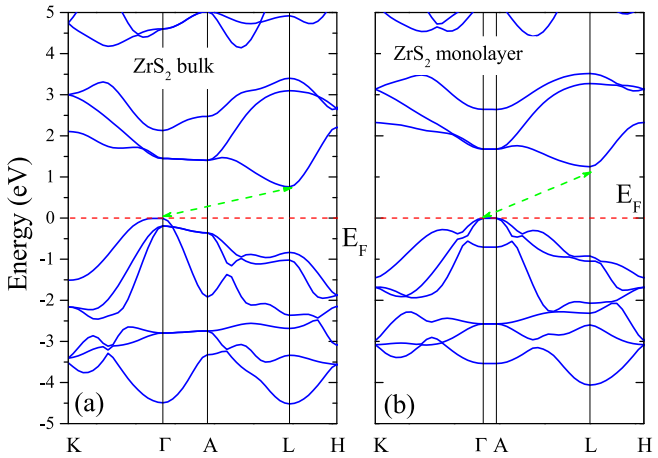

Fig. 2. Band structures of bulk (a) and monolayer (b) ZrS_2, respectively, where the Fermi level is shifted to zero.

lower peaks, improving the light absorption of monolayer ZrS_2, since there are more inter-band transitions than those in bulk ZrS_2. Our calculated band gaps for the bulk and monolayer ZrS_2, respectively, are 0.750 eV and 1.248 eV, which are in good agreement with the available GGA theoretical reports [48,51]. However, the lack of Hartree-Fock exchange-correlation may lead to under-estimated band gap of monolayer in comparison with experimental values [52–54].The band gap of ZrS_2 monolayer is close to 2 eV, which is very suitable for absorption of light. The disagreements between the results of DFT calculations should not indicate any failures or shortfalls of DFT [55]. The trend of material's behavior should not change. Moreover, the APW + lo method is proven to reproduce reliable electronic and optical properties of materials [56,57].

Fig. 3(a and b) shows that the valence band of the ZrS_2 is mainly contributed by sulfur *s*-state at the first peak with energy level ranging from −13 eV to −11 eV. In addition, we find that an energy gap of about 6 eV between the first and the second peaks is related to the sulfur *p*-state in the energy range of (−3.5÷0) eV. At the same time, these states are also mixed with substantial portion of zirconium *s/p/d*-states. This suggests that the Zr−S is strong covalent bond. Whereas, the conduction band is contributed by major part of unoccupied zirconium *d*-orbital, which is separated into two different peaks. The highest peak of zirconium at the energy of 3 eV separates itself into one more lower peak at 1.5 eV owing to the distortion at octahedral position of zirconium atom [59]. This effect becomes more obvious in monolayer ZrS_2 with shaper peak separation. The mixing between the zirconium *s*, *d* and *p* states in conduction band leads to a decrease in band gap energy, especially in bulk ZrS_2 with more sheets of Zr atoms, leading to a lower band gap in bulk ZrS_2 in comparison with that in monolayer.

3.2. Optical properties of ZrS_2 bulk and monolayer

We further consider the optical behavior of the bulk and monolayer ZrS_2. It is obvious that the change in the band gap and electronic structure of bulk and monolayer affects the ability of ZrS_2 to absorb sunlight for solar cell application. This raises an

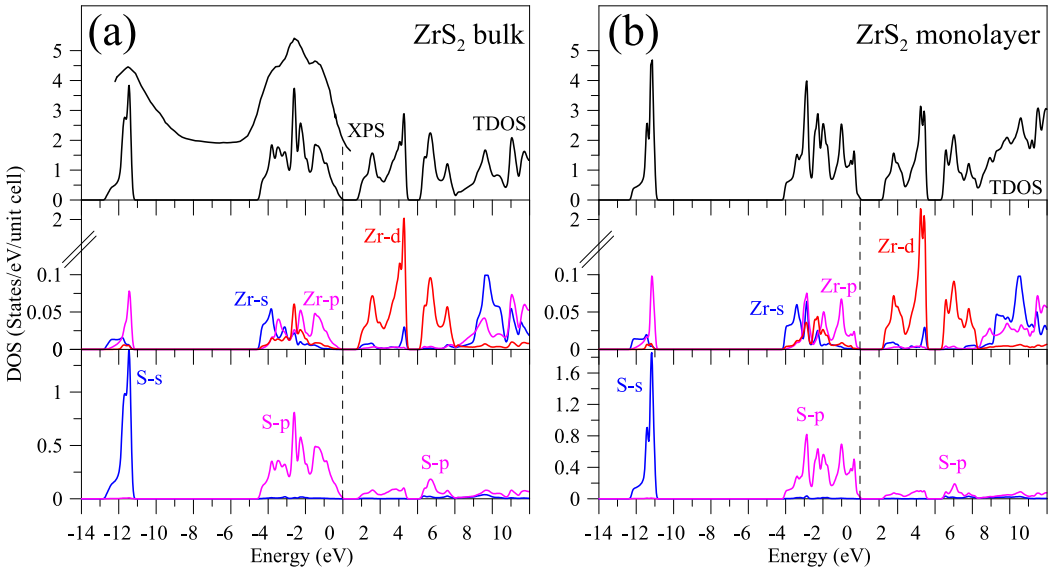

Fig. 3. Total DOS and main partial densities of bulk (a) and monolayer (b) ZrS_2, respectively. The XPS valence-band spectrum from Ref. [58] is plotted by the same energy scale with the TDOS of bulk ZrS_2.

interest of studying their optical properties. The structure of ZrS_2 is hexagonal, so we estimate the optical spectra responding to two components of the incident electrical field which is perpendicular (E⊥z) and parallel (E||z) to the z direction of the crystal.

The real $\varepsilon_1(\omega)$ and imaginary $\varepsilon_2(\omega)$ components of dielectric function represent the ability of material to store energy and the energy loss. The dielectric function is calculated based on the momentum representation which considers the eigenvalue energy E_{kn} corresponding to the crystal momentum k and spin σ, the frequency ω of the incident electromagnetic wave, the mass m and charge e of electron [60].

$$\varepsilon_2^{ij}(\omega) = \frac{4\pi^2 e^2}{Vm^2\varpi^2} \times \sum_{nn'\sigma} \langle kn\sigma|p_i|kn'\sigma\rangle\langle kn'\sigma|p_j|kn\sigma\rangle \times f_{kn}(1 - f_{kn'})\delta(E_{kn'} - E_{kn} - \hbar\omega) \tag{1}$$

where V is the unit-cell volume, p is the momentum operator, $|knp\rangle$ is the wave function of the crystal, and f_{kn} is the Fermi distribution function counting only the transitions of material from occupied state to unoccupied one.

The real component of complex permittivity can be obtained based on $\varepsilon_2(\omega)$ by using Kramers-Kronig formula [61]:

$$\varepsilon_1(\omega) = 1 + \frac{2}{\pi}P\int_0^\infty \frac{\omega'\varepsilon_2(\omega')}{\omega'^2 - \omega^2}d\omega' \tag{2}$$

where P is the principal value of the integral.

Fig. 4(a) and Fig. 4(b) show similar trend of $\varepsilon_1(\omega)$ for both bulk and monolayer ZrS_2. The real component plays main role in the dielectric function of the material at equilibrium state. The $\varepsilon_1(\omega)$ of the two compounds reaches its highest values with three main peaks E1, E2, and E3 in the following energy ranges (1÷2.8) eV, (2.8÷4) eV and (4÷10) eV. This indicates that ZrS_2 based compounds have reflectivity of high energy photon. The $\varepsilon_1(\omega)$ decreases from its highest peak E1 to a non-significant peak E4 at 12 eV and stabilizes at the energy level greater than 14 eV. The green experimental line for $\varepsilon_1(\omega)$ in Fig. 4(a) shows good agreement between the theoretical and experimental results. For the energy level below 14 eV, the material has anisotropic behavior which is reflected by the difference in value of $\varepsilon_1(\omega)$ by in-plane E⊥z and out-plane E||z directions. At the energy intervals (2.8÷4) eV and (4÷10) eV, the $\varepsilon_1(\omega)$of monolayer ZrS_2 has significant decrease between two top values corresponding to the separation of each of the $\varepsilon_1(\omega)$ peaks E2, and E3 into two narrower peaks.

The imaginary component $\varepsilon_2(\omega)$ in Fig. 4(c) and Fig. 4(d) shows similar respond of bulk and monolayer ZrS_2 to the medium. The $\varepsilon_2(\omega)$ peaks at energy level from 2 to 8 eV correspond to the inter-band transitions in Fig. 3, which happens between sulfur p-state, zirconium $s/p/d$-state in valence band and the zirconium d-state in conduction band. The peaks at energy level above 8 eV originate from inter-band transitions mainly between sulfur s-state, zirconium s/p-state in valence band and zirconium d-state in conduction band. The highest peak of $\varepsilon_2(\omega)$ at the low energy range 1.5–2.5 eV indicates that the loss energy happens at low energy. At this energy range we also observe strong anisotropy in the behavior of $\varepsilon_2(\omega)$ reflected by significant difference between E⊥z and E||z. The reflectivity increases with the gradual decreasing of $\varepsilon_2(\omega)$ peaks which become null at energy higher than 13 eV. In comparison with Fig. 4(b) for monolayer ZrS_2, we see that the valence band has two more peaks along the A-Γ path relating to the separation of each of the two peaks E2 (3.5–7 eV) and E3 (7.5–11 eV) into two peaks, indicating that monolayer is more sensitive to the medium.

This leads to the interest of investigating the adsorption coefficient $\alpha(\omega)$, optical reflectance $R(\omega)$, and the energy loss $L(\omega)$ of bulk and monolayer ZrS_2, which are calculated as following [63]:

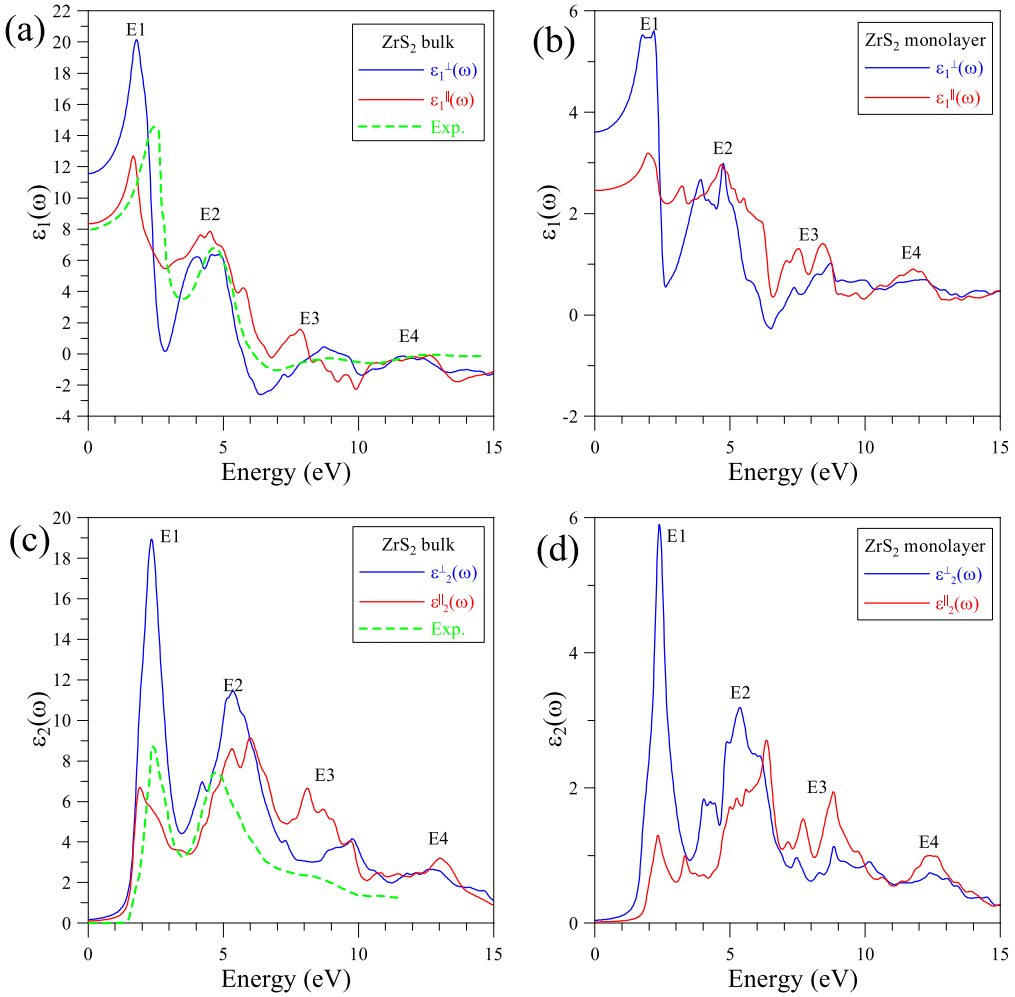

Fig. 4. The real $\varepsilon_1(\omega)$ and imaginary $\varepsilon_2(\omega)$ component of the dielectric function in bulk (a, c) and in monolayer (b, d) ZrS_2 calculated along x- (blue line) and along z- (red line) axes, experimental permittivity from Ref. [62] (dot lines) for the case of bulk ZrS_2.

$$\alpha^{ij}(\omega) = \frac{2\omega k^{ij}(\omega)}{c} \tag{3}$$

$$R^{ij}(\omega) = \frac{(n^{ij}-1)^2 + k^{ij^2}}{(n^{ij}-1)^2 - k^{ij^2}} = \left|\frac{\sqrt{\varepsilon_1^{ij} + i\varepsilon_2^{ij}} - 1}{\sqrt{\varepsilon_1^{ij} + i\varepsilon_2^{ij}} + 1}\right|^2 \tag{4}$$

$$L^{ij}(\omega) = -Im(\varepsilon^{-1})^{ij} = \frac{\varepsilon_2^{ij}(\omega)}{\varepsilon_1^{ij}(\omega)^2 + \varepsilon_2^{ij}(\omega)^2} \tag{5}$$

where n^{ij} and k^{ij} are the extinction and refraction index respectively, these indexes are calculated as follows:

$$n^{ij}(\omega) = \frac{1}{\sqrt{2}}\left[\sqrt{\varepsilon_1^{ij}(\omega)^2 + \varepsilon_2^{ij}(\omega)^2} + \varepsilon_1^{ij}(\omega)\right]^{\frac{1}{2}} \tag{6}$$

$$k^{ij}(\omega) = \frac{1}{\sqrt{2}}\left[\sqrt{\varepsilon_1^{ij}(\omega)^2 + \varepsilon_2^{ij}(\omega)^2} - \varepsilon_1^{ij}(\omega)\right]^{\frac{1}{2}} \tag{7}$$

Fig. 5 shows that the absorption begins at visible light with energy ranging from 1.5 eV to its local peak at the yellow color of about 2.5 eV. Then it increases with higher peaks in the region of UV light and reaches the highest value at $106 \times 10^4\,cm^{-1}$. This optical behavior of the two compounds makes ZrS_2 a promising photovoltaic material. The first and second absorption peaks directly relate to the surface plasmon resonance in Fig. 3 the lowest negative values of $\varepsilon_1(\omega)$ at 3 eV and 5.2 eV. Despite of the fact that $\alpha(\omega)$ depends on both $\varepsilon_1(\omega)$ and $\varepsilon_2(\omega)$, the anisotropy is not significant for bulk ZrS_2 over the whole absorption range, while in the case of monolayer structure, this anisotropy becomes prominent at the ultraviolet regions 8–11 eV and 11.5–14.5 eV. The sharp peaks in

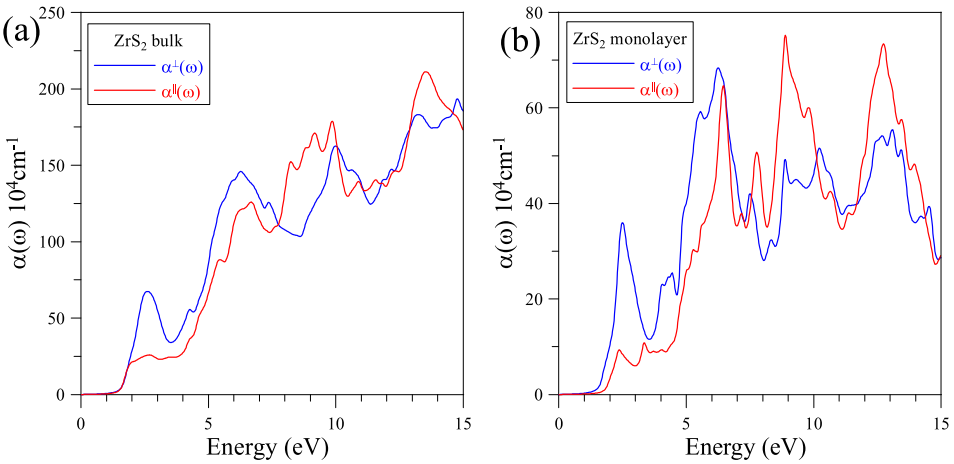

Fig. 5. The absorption coefficient $\alpha(\omega)$ of bulk (a) and monolayer (b) ZrS_2 calculated along x-axis (blue curve) and z-axis (red curve).

ultraviolet–visible absorption spectroscopy propose monolayer ZrS_2 to be good material for sensor application.

It can be seen in Fig. 6 that both the refractive index $n(\omega)$ and extinction coefficient $k(\omega)$ in bulk and monolayer zirconium sulfide fluctuate over whole energy level ranging from 0 eV to 15 eV. Anisotropy is observed at energy lower than 10 eV for bulk, while in monolayer it occurs at energy lower than 7 eV.

Fig. 7(a) and Fig. 7(b) show a pattern of energy loss which has a clear relationship with the imaginary component $\varepsilon_2(\omega)$ of

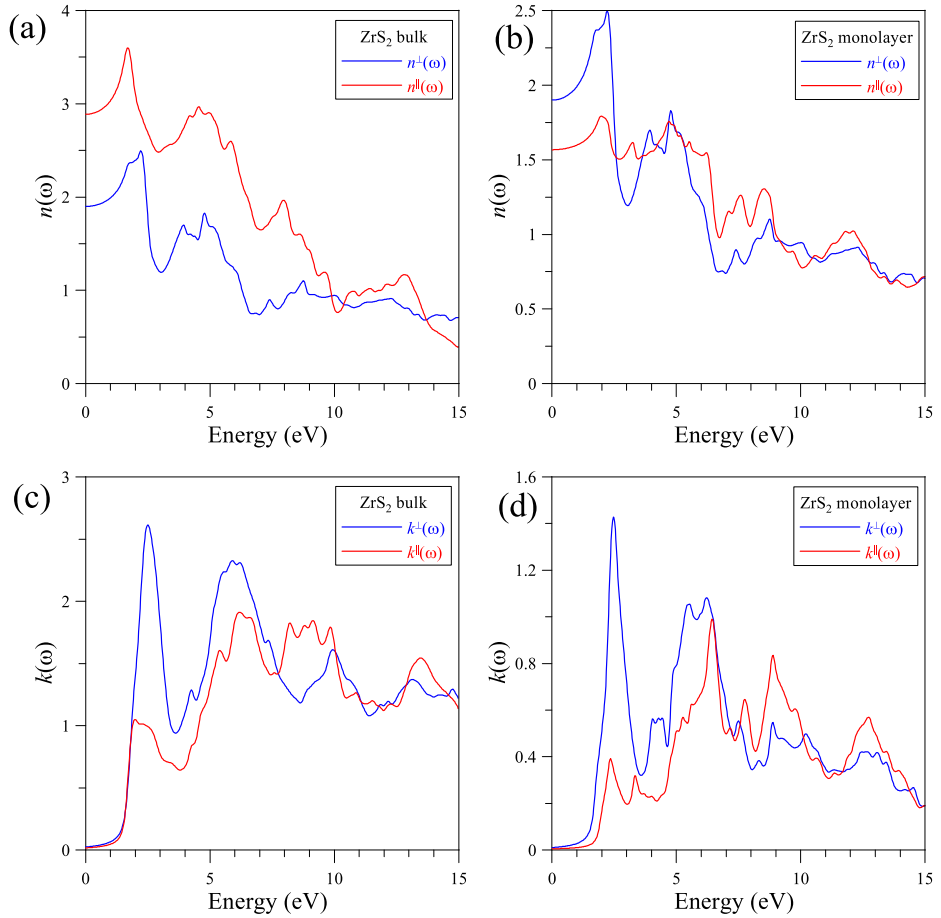

Fig. 6. The refractive index $n(\omega)$(a, b) and extinction coefficient $k(\omega)$(c, d) of bulk and monolayer ZrS_2 calculated along x- (blue line) and along z- (red line) axes.

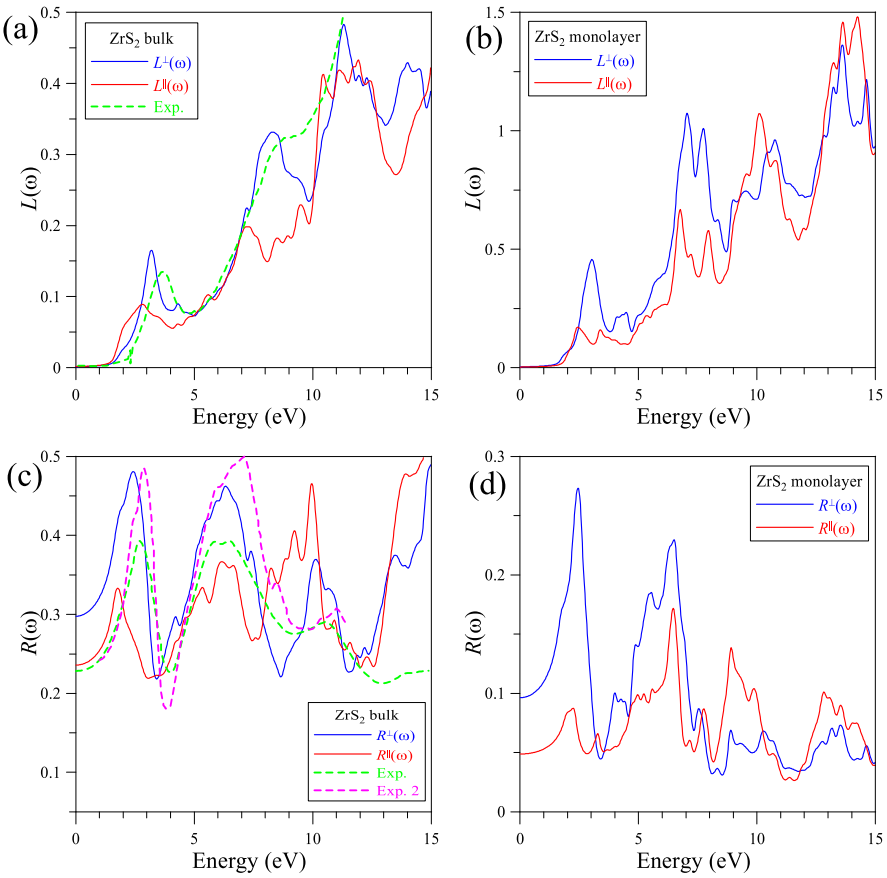

Fig. 7. The energy loss $L(\omega)$ and the reflectance $R(\omega)$ of bulk ZrS_2 (a, c) and of monolayer ZrS_2 (b, d) calculated along x- (blue line) and along z- (red line) axes, the experimental data for energy loss $L(\omega)$ [64] and the reflectance $R(\omega)$ [37,62] (dot lines) for the case of bulk ZrS_2.

dielectric function shown in Fig. 3(c) and Fig. 3(d). In bulk ZrS_2, the value of energy loss along the out-plane direction is close to the experimental data [64]. The first peak appears at the energy of about 3.3 eV, at this peak, the difference between calculated value and experimental value is about 0.4. The highest peak appears at the energy of 11.4 eV, both our calculation and the experiment show the energy loss of about 0.8. The energy loss along the x-axis in bulk ZrS_2 has lower peaks in comparison with the z-axis. The monolayer ZrS_2 in Fig. 7(b), as expected from the previous results of $\varepsilon_1(\omega)$, responds better to the external field. The energy loss peaks are shaper and with higher value in comparison with the bulk. The first peak by x-axis is at 3.2 eV, while at this energy level the peak along z-axis is not significant. However, when the energy is higher than 7 eV, the peaks along two direction are getting closer to each other. The highest peak is at about 14 eV. The energy loss pattern in Fig. 7(b) show that monolayer ZrS_2 can result in better plasmon resonance than the bulk.

The reflectivity $R(\omega)$ of bulk and monolayer ZrS_2 in Fig. 7(c and d) are fluctuated curves over the whole energy range 0–15 eV, which have local maxima and minima at the energy levels corresponding to the maxima and minima of $\varepsilon_2(\omega)$ in Fig. 3. For bulk ZrS_2, the reflectivity starts with 20 %–30 % at 0 eV, at the energy level higher than 1 eV, the reflectivity remains the same at the rate of about 50 %. Its interesting that the reflectivity of bulk ZrS_2 to the photon energy ranging from visible to mid-ultraviolet are in good agreement with experimental data [37,62]. The monolayer ZrS_2 has smaller $R(\omega)$ starting at 5 % to 10 % then it reaches the highest value of 25 % at the energy level about 2.3 eV (the highest level of $\varepsilon_2(\omega)$ for monolayer in Fig. 3(d)), and decreases gradually with lower local peaks. The strong anisotropy in both configurations confirms the semi-conductivity property of the ZrS_2-based materials.

4. Conclusion

In conclusion, we apply the APW + lo method to study bulk and monolayer zirconium sulfide. At the energy ranging from 0 eV to 14 eV, our calculation is in good agreement with experimental data for dielectric function, absorption rate, and loss energy. Zirconium sulfide is an indirect bandgap semiconductor with the band gap energy from 1.2 eV to 2 eV. The strong hybridization of sulfur 3-*p* orbital and zirconium 3-*d* orbital confirms the strong covalent bond between Zr and S atoms. At energy below 10 eV, the ZrS_2-based compounds have strong anisotropic optical behavior. The dielectric function shows that zirconium sulfide has reflectivity at high energy. Zirconium sulfide has best light absorption in the region of visible light to mid-ultraviolet wave length. The monolayer zirconium inherits familiar electronic and optical behaviors of bulk zirconium. At the same time, the 2D compound also exhibits its

own perspective properties in photovoltaic material with optimal energy band gap near 2 eV, in sensor application with more peaks at the valence band maximum and sharper peaks of absorption curve. Furthermore, the loss energy in the 2D zirconium is even higher than the one in bulk structure, this suggests a promising material for plasmon application.

References

[1] A.H. Castro Neto, F. Guinea, N.M.R. Peres, K.S. Novoselov, A.K. Geim, The electronic properties of graphene, Rev. Mod. Phys. 81 (1) (2009) 109–162.
[2] A.K. Geim, K.S. Novoselov, The rise of graphene, Nat. Mater. 6 (2007) 183–191.
[3] M. Sun, Q. Ren, Y. Zhao, J.-P. Chou, J. Yu, W. Tang, Electronic and magnetic properties of 4d series transition metal substituted graphene: a first-principles study, Carbon 120 (2017) 265–273.
[4] L. Mochalov, D. Dorosz, A. Nezhdanov, M. Kudryashov, S. Zelentsov, D. Usanov, A. Logunov, A. Mashin, D. Gogova, Investigation of the composition-structure-property relationship of As_xTe^{100-x} films prepared by plasma deposition, Spectrochim. Acta Mol. Biomol. Spectrosc. 191 (2018) 211–216.
[5] L. Mochalov, A. Nezhdanov, A. Logunov, M. Kudryashov, I. Krivenkov, A. Vorotyntsev, D. Gogova, A. Mashin, Optical emission of two-dimensional arsenic sulfide prepared by plasma, Superlattice. Microst. 114 (2018) 305–313.
[6] L. Mochalov, M. Kudryashov, A. Logunov, S. Zelentsov, A. Nezhdanov, A. Mashin, D. Gogova, G. Chidichimo, G. De Filpo, Structural and optical properties of arsenic sulfide films synthesized by a novel pecvd-based approach, Superlattice. Microst. 111 (2017) 1104–1112.
[7] W. Choi, N. Choudhary, G.H. Han, J. Park, D. Akinwande, Y.H. Lee, Recent development of two-dimensional transition metal dichalcogenides and their applications, Mater. Today 20 (3) (2017) 116–130.
[8] S. Li, M. Sun, J.-P. Chou, J. Wei, H. Xing, A. Hu, First-principles calculations of the electronic properties of SiC-based bilayer and trilayer heterostructures, Phys. Chem. Chem. Phys. 20 (2018) 24726–24734.
[9] M. Sun, Q. Ren, S. Wang, J. Yu, W. Tang, Electronic properties of janus silicene: new direct band gap semiconductors, J. Phys. D Appl. Phys. 49 (44) (2016) 445305.
[10] M. Sun, J.-P. Chou, J. Yu, W. Tang, Effects of structural imperfection on the electronic properties of graphene/WSe_2 heterostructures, J. Mater. Chem. C 5 (39) (2017) 10383–10390.
[11] H. Schmidt, F. Giustiniano, G. Eda, Electronic transport properties of transition metal dichalcogenide field-effect devices: surface and interface effects, Chem. Soc. Rev. 44 (21) (2015) 7715–7736.
[12] F. Schwierz, J. Pezoldt, R. Granzner, Two-dimensional materials and their prospects in transistor electronics, Nanoscale 7 (18) (2015) 8261–8283.
[13] M. Sun, J.-P. Chou, Q. Ren, Y. Zhao, J. Yu, W. Tang, Tunable Schottky barrier in van der waals heterostructures of graphene and g-GaN, Appl. Phys. Lett. 110 (17) (2017) 173105.
[14] L. Jaekwang, H. Jingsong, G.S. Bobby, Y. Mina, Strain-engineered optoelectronic properties of 2D transition metal dichalcogenide lateral heterostructures, 2D Mater. 4 (2) (2017) 021016.
[15] P. Johari, V.B. Shenoy, Tuning the electronic properties of semiconducting transition metal dichalcogenides by applying mechanical strains, ACS Nano 6 (6) (2012) 5449–5456.
[16] T. Shen, A.V. Penumatcha, J. Appenzeller, Strain engineering for transition metal dichalcogenides based field effect transistors, ACS Nano 10 (4) (2016) 4712–4718.
[17] W. Wei, Y. Dai, C. Niu, B. Huang, Controlling the electronic structures and properties of in-plane transition-metal dichalcogenides quantum wells, Sci. Rep. 5 (2015) 17578.
[18] H. Wang, H. Yuan, S. Sae Hong, Y. Li, Y. Cui, Physical and chemical tuning of two-dimensional transition metal dichalcogenides, Chem. Soc. Rev. 44 (9) (2015) 2664–2680.
[19] H. Zhai, Z. Qin, D. Sun, J. Wang, C. Liu, N. Min, Q. Li, Pressure-induced phase transition, metallization and superconductivity in ZrS_2, Phys. Chem. Chem. Phys. 20 (36) (2018) 23656–23663.
[20] A. Kuc, T. Heine, The electronic structure calculations of two-dimensional transition-metal dichalcogenides in the presence of external electric and magnetic fields, Chem. Soc. Rev. 44 (9) (2015) 2603–2614.
[21] F. Liu, J. Zhou, C. Zhu, Z. Liu, Electric field effect in two-dimensional transition metal dichalcogenides, Adv. Funct. Mater. 27 (19) (2016) 1602404.
[22] M. Sharma, A. Kumar, P.K. Ahluwalia, R. Pandey, Strain and electric field induced electronic properties of two-dimensional hybrid bilayers of transition-metal dichalcogenides, J. Appl. Phys. 116 (6) (2014) 063711.
[23] Z. Zeng, Z. Yin, X. Huang, H. Li, Q. He, G. Lu, F. Boey, H. Zhang, Single-layer semiconducting nanosheets: high-yield preparation and device fabrication, Angew. Chem. Int. Ed. 50 (47) (2011) 11093–11097.
[24] L. Li, X. Fang, T. Zhai, M. Liao, U.K. Gautam, X. Wu, Y. Koide, Y. Bando, D. Golberg, Electrical transport and high-performance photoconductivity in individual ZrS_2 nanobelts, Adv. Mater. 22 (37) (2010) 4151–4156.
[25] L. Li, H. Wang, X. Fang, T. Zhai, Y. Bando, D. Golberg, High-performance Schottky solar cells using ZrS_2 nanobelt networks, Energy Environ. Sci. 4 (7) (2011) 2586–2590.
[26] Y. Wen, Y. Zhu, S. Zhang, Low temperature synthesis of ZrS_2 nanoflakes and their catalytic activity, RSC Adv. 5 (81) (2015) 66082–66085.
[27] H.L. Zhuang, R.G. Hennig, Computational search for single-layer transition-metal dichalcogenide photocatalysts, J. Phys. Chem. C 117 (40) (2013) 20440–20445.
[28] G. Fiori, F. Bonaccorso, G. Iannaccone, T. Palacios, D. Neumaier, A. Seabaugh, S.K. Banerjee, L. Colombo, Electronics based on two-dimensional materials, Nat. Nanotechnol. 9 (2014) 768.
[29] H.-P. Komsa, A.V. Krasheninnikov, Electronic structures and optical properties of realistic transition metal dichalcogenide heterostructures from first principles, Phys. Rev. B 88 (8) (2013) 085318.
[30] M. Moustafa, T. Zandt, C. Janowitz, R. Manzke, Growth and band gap determination of the ZrS_xSe_{2-x} single crystal series, Phys. Rev. B 80 (3) (2009) 035206.
[31] H. Yan, X. Wang, M. Yao, X. Yao, Band structure design of semiconductors for enhanced photocatalytic activity: the case of TiO_2, Prog. Nat. Sci.: Mater. Int. 23 (4) (2013) 402–407.
[32] B. Radisavljevic, A. Radenovic, J. Brivio, V. Giacometti, A. Kis, Single-layer MoS_2 transistors, Nat. Nanotechnol. 6 (2011) 147.
[33] J. Kang, S. Tongay, J. Zhou, J. Li, J. Wu, Band offsets and heterostructures of two-dimensional semiconductors, Appl. Phys. Lett. 102 (1) (2013) 012111.
[34] X. Zhang, Z. Meng, D. Rao, Y. Wang, Q. Shi, Y. Liu, H. Wu, K. Deng, H. Liu, R. Lu, Efficient band structure tuning, charge separation, and visible-light response in ZrS_2-based van der waals heterostructures, Energy Environ. Sci. 9 (3) (2016) 841–849.
[35] Y. Li, J. Kang, J. Li, Indirect-to-direct band gap transition of the ZrS_2 monolayer by strain: first-principles calculations, RSC Adv. 4 (15) (2014) 7396–7401.
[36] H.Y. Lv, W.J. Lu, D.F. Shao, H.Y. Lu, Y.P. Sun, Strain-induced enhancement in the thermoelectric performance of a ZrS_2 monolayer, J. Mater. Chem. C 4 (20) (2016) 4538–4545.
[37] D.L. Greenaway, R. Nitsche, Preparation and optical properties of group IV-VI_2 chalcogenides having the CdI_2 structure, J. Phys. Chem. Solid. 26 (9) (1965) 1445–1458.
[38] S. Li, C. Wang, H. Qiu, Single- and few-layer ZrS_2 as efficient photocatalysts for hydrogen production under visible light, Int. J. Hydrogen Energy 40 (45) (2015) 15503–15509.
[39] S. Jimin, H. Le, W. Zhongming, Effects of vertical electric field and compressive strain on electronic properties of bilayer ZrS_2, J. Semiconduct. 38 (3) (2017) 033001.
[40] L. Ao, A. Pham, H.Y. Xiao, X.T. Zu, S. Li, Theoretical prediction of long-range ferromagnetism in transition-metal atom-doped d0 dichalcogenide single layers SnS_2 and ZrS_2, Phys. Chem. Chem. Phys. 18 (36) (2016) 25151–25160.

[41] B. Krishnakumar, T. Imae, J. Miras, J. Esquena, Synthesis and azo dye photodegradation activity of ZrS_2ZnO nano-composites, Separ. Purif. Technol. 132 (2014) 281–288.
[42] Y. Si, H.-Y. Wu, H.-M. Yang, W.-Q. Huang, K. Yang, P. Peng, G.-F. Huang, Dramatically enhanced visible light response of monolayer ZrS_2 via non-covalent modification by double-ring tubular B20 cluster, Nanoscale Res. Lett. 11 (1) (2016) 495.
[43] X. Zhao, P. Chen, C. Yang, X. Zhang, S. Wei, Electronic and magnetic properties of the n monodoping and (Mn, N)-codoped ZrS_2, J. Mater. Sci. 53 (10) (2018) 7466–7474.
[44] P. Blaha, K. Schwarz, G.K.H. Madsen, D. Kvasnicka, J. Luitz, R. Laskowski, F. Tran, L.D. Marks, WIEN2k, an Augmented Plane Wave + Local Orbitals Program for Calculating Crystal Properties, Karlheinz Schwarz, Techn. Universitt Wien, Austria, 2018.
[45] J. P. Perdew, K. Burke, M. Ernzerhof, Generalized gradient approximation made simple, Phys. Rev. Lett. 77 (18).
[46] J.P. Perdew, K. Burke, M. Ernzerhof, Generalized gradient approximation made simple, Phys. Rev. Lett. 77 (3865) (1996) Physical Review Letters 78 (7) (1997) 1396–1396.
[47] P.E. Blöchl, O. Jepsen, O.K. Andersen, Improved tetrahedron method for brillouin-zone integrations, Phys. Rev. B 49 (23) (1994) 16223.
[48] A. Kumar, H. He, R. Pandey, P.K. Ahluwalia, K. Tankeshwar, Semiconductor to metal phase transition in monolayer ZrS_2: GGA + U study, AIP Conf. Proc. 1665 (1) (2015) 090016.
[49] Q. Zhao, Y. Guo, K. Si, Z. Ren, J. Bai, X. Xu, Elastic, electronic, and dielectric properties of bulk and monolayer ZrS_2, $ZrSe_2$, HfS_2, $HfSe_2$ from van der waals density-functional theory, Phys. Status Solidi 254 (9) (2017) 1700033.
[50] A. Kumar, H. He, R. Pandey, P.K. Ahluwalia, K. Tankeshwar, Pressure and electric field-induced metallization in the phase-engineered ZrX_2 (X = S, Se, Te) bilayers, Phys. Chem. Chem. Phys. 17 (29) (2015) 19215–19221.
[51] Q. Xin, X. Zhao, X. Ma, N. Wu, X. Liu, S. Wei, Electronic structure in 1T-ZrS_2 monolayer by strain, Phys. E Low-dimens. Syst. Nanostruct. 93 (2017) 87–91.
[52] J.L.F. Da Silva, M.V. Ganduglia-Pirovano, J. Sauer, V. Bayer, G. Kresse, Hybrid functionals applied to rare-earth oxides: the example of ceria, Phys. Rev. B 75 (2007) 045121.
[53] A. Janotti, J.B. Varley, P. Rinke, N. Umezawa, G. Kresse, C.G. Van de Walle, Hybrid functional studies of the oxygen vacancy in TiO_2, Phys. Rev. B 81 (2010) 085212.
[54] J. Muscat, A. Wander, N. Harrison, On the prediction of band gaps from hybrid functional theory, Chem. Phys. Lett. 342 (3) (2001) 397–401.
[55] D. Bagayoko, Understanding density functional theory (DFT) and completing it in practice, AIP Adv. 4 (12) (2014) 127104.
[56] D.Q. Khoa, C.V. Nguyen, H.V. Phuc, V.V. Ilyasov, T.V. Vu, N.Q. Cuong, B.D. Hoi, D.V. Lu, E. Feddi, M. El-Yadri, M. Farkous, N.N. Hieu, Effect of strains on electronic and optical properties of monolayer SnS: Ab-initio study, Phys. B Condens. Matter 545 (2018) 255–261.
[57] H. Khachai, R. Khenata, A. Bouhemadou, A. Haddou, H.R. Ali, B. Amrani, D. Rached, B. Soudini, Fp-apw + lo calculations of the electronic and optical properties of alkali metal sulfides under pressure, J. Phys. Condens. Matter 21 (9) (2009) 095404.
[58] H. Isomäki, J. v. Boehm, Bonding and band structure of ZrS_2 and $ZrSe_2$, Phys. Scripta 24 (2) (1981) 465.
[59] Y.S. Kim, H.C. Ko, H.S. Park, Electronic structure and chemical bonding of zirconium disulfide, Met. Mater. 6 (3) (2000) 177–180.
[60] C. Ambrosch-Draxl, J.O. Sofo, Linear optical properties of solids within the full-potential linearized augmented planewave method, Comput. Phys. Commun. 175 (1) (2006) 1–14.
[61] F. Wooten, Optical Properties of Solids, Academic, New York, 1972.
[62] H. Isomäki, J. von Boehm, Optical properties of ZrS_2, Phys. B + C 105 (1) (1981) 156–158.
[63] T.V. Vu, A.A. Lavrentyev, B.V. Gabrelian, O.V. Parasyuk, V.A. Ocheretova, O.Y. Khyzhun, Electronic structure and optical properties of $Ag_2HgSnSe_4$: first-principles dft calculations and x-ray spectroscopy studies, J. Alloy. Comp. 732 (2018) 372–384.
[64] M.G. Bell, W.Y. Liang, Electron energy loss studies in solids; the transition metal dichalcogenides, Adv. Phys. 25 (1) (1976) 53–86.